Pergamon

Int. J. Heat Mass Transfer. Vol. 37, Suppl. 1, pp. 31–40, 1994
Copyright © 1994 Elsevier Science Ltd
Printed in Great Britain. All rights reserved
0017-9310/94 $6.00 + 0.00

0017-9310(93)E0062-L

Analysis of post-CHF swirl flow heat transfer

D. M. FRANCE, W. J. MINKOWYCZ and C. CHANG

The University of Illinois at Chicago, Department of Mechanical Engineering (M/C 251), 842 W. Taylor Street, Chicago, IL 60607, U.S.A.

Abstract—A thermodynamic nonequilibrium model has been developed for a two-phase, vapor and liquid-drop, dispersed swirl flow in a vertical tube with a twisted-tape insert. The solution of the nonlinear differential equations proceeds from the critical heat flux location downstream through the post-CHF region. Wall temperature, superheat vapor temperature, heat transfer rates to the phases, and phase velocity distributions are predicted. Results were verified by comparison with experimental data from a heat exchanger application with high pressure (16.0 MPa) boiling water heated by a flowing liquid. The resulting low wall-superheat data used in this study were in the mass flux range of 910–1878 kg m^{-2} s^{-1} with tape-twist ratios of 2.51, 5.02 and 7.53 based on 180° of twist. Model predictions are presented for parameters not measured experimentally which lend insight into post-CHF heat transfer under swirl flow conditions.

INTRODUCTION

SYSTEMS that boil a fluid to saturated or superheated vapor can potentially benefit from heat transfer augmentation. Investigations into heat transfer augmentation for single-phase flow are numerous, but two-phase flow studies are few by comparison. Applications for augmented two-phase flow heat transfer include refrigeration/air-conditioning evaporators, electric power plant steam generators, and general industrial boilers.

An augmentation method that is attractive for heat exchanger applications imposes a swirl flow component on the boiling fluid. An important two-phase flow regime for such heat exchanger application is the post-CHF region. Here the heat transfer coefficients are considerably lower than the bubbly, slug or annular flow regimes occurring upstream of the critical heat flux (CHF). Of specific interest to this investigation is the post-CHF regime where swirl flow is generated by twisted-tape inserts inside of tubes.

The majority of previous investigations in the post-CHF regime of two-phase heat transfer have been related to axial flow conditions. In addition, the large majority of data in the engineering literature including both axial and swirl flows in the post-CHF region were obtained under the condition of high wall-superheat, whereas low wall-superheat is indicative of many heat exchangers employing convection heating. The high superheat data for both axial and swirl flows have shown a weak contribution to the heat transfer resulting from the direct interaction of the drops with the heated tube walls. However, recent low wall-superheat data [1, 2] indicate an increase in importance in this mechanism.

Initial work on the prediction of heat transfer to pipe flow augmented by twisted-tape inserts in the post-CHF region was due to Bergles *et al.* [3]. The database for the heat transfer correlation developed was boiling nitrogen near atmospheric pressure with a low reduced pressure of 0.045, two tape-twist ratios ($Y = 4.1$ and $Y = 8.5$), low mass fluxes of 30–140 kg m^{-2} s^{-1}, and relatively high wall-superheats of 60–300°C. These parameters are outside of the range of many heat exchanger applications of the type mentioned. The objective of this study was to develop a broader-based prediction method for post-CHF heat transfer with twisted-tape-induced swirl flow. The approach was to verify the model with experimental data [4] obtained from high-pressure boiling water with twisted-tape-induced swirl flow.

MODEL

A thermodynamic nonequilibrium model was developed for two-phase, vapor and liquid-drops, dispersed swirl flow in a vertical tube with twisted-tape inserts. Heat transfer phenomena were included between the two phases and between each phase and the solid boundary where a variable heat flux was imposed in the axial z direction. This heat flux boundary condition allowed comparison with data [4]. The principles of conservation of mass, momentum and energy were applied to the total mixture and to the drops separately. The hydrodynamic behavior of the drops was represented by a mean drop size that initiated at CHF with a diameter based on a critical Weber number criterion. The axial phase velocities in the z direction are denoted u_l and u_v for the liquid drops and the vapor. A second subscript, θ or s, corresponds to the tangential and resultant (streamline) velocities, respectively.

Conservation of mass

The mass flow rates of the two phases are defined as

NOMENCLATURE

a swirl acceleration [m s^{-2}]
A cross-sectional flow area [m^2]
C_D drag coefficient for a single sphere
c_p specific heat [kJ kg^{-1} °C^{-1}]
d drop diameter [m]
D flow duct diameter [m]
D_h hydraulic diameter [m]
f Fanning friction factor
f_{lt} Fanning friction factor if the total flow were liquid
F drop-wall heat transfer parameter
g gravitational acceleration [m s^{-2}]
G mass flux [kg m^{-2} s^{-1}]
h heat transfer coefficient [kW m^{-2} °C^{-1}]
i_{lv} latent heat of vaporization [kJ kg^{-1}]
J_i generalized parameter
J_i' $d(J_i)/dz$
k thermal conductivity [kW m^{-1} °C^{-1}]
N drop number density [m^{-3}]
P pressure [kPa]
P_R reduced pressure
Pr Prandtl number
q'' heat flux [kW m^{-2}]
R_s twisted-tape swirl parameter
Re Reynolds number, based on D_h
S velocity slip ratio, u_v/u_l
T temperature [°C]
u velocity [m s^{-1}]
W mass flow rate [kg s^{-1}]
X actual vapor mass quality
X_{eq} equilibrium vapor mass quality
Y tape-twist ratio, (length of 180° of twist)/D
z axial length [m].

Greek symbols
α void fraction
β coefficient of volumetric thermal expansion [K^{-1}]
η evaporation force parameter
μ dynamic viscosity [kg m^{-1} s^{-1}]
ρ density [kg m^{-3}]
σ surface tension [N m^{-1}]
φ_l liquid volume fraction
Φ_{lo}^2 two-phase friction multiplier relative to total flow of liquid.

Subscripts
l liquid
ls swirl flow of liquid
m two-phase mixture
s swirl (streamline flow direction)
sat saturation
v vapor
w wall
l–v vapor to drop
l–w wall to drop
v–w wall to vapor
θ tangential flow direction.

$$W_v = \rho_v u_v (1-\varphi_l) A \tag{1}$$

and

$$W_l = \rho_l u_l \varphi_l A, \tag{2}$$

where ρ_v and ρ_l are phase (material) densities, and φ_l is the liquid volume fraction at any axial position z in the flow duct. Because of the dispersed structure of the flow, it is convenient to use the liquid volume fraction explicitly in the model rather than the vapor volume fraction (void fraction). The mass fluxes of each phase are defined as the phase mass flow rates divided by the total duct cross-sectional area A. For constant A, the conservation of mass for the mixture in terms of mass fluxes is

$$G = G_v + G_l = \text{constant}, \tag{3}$$

where the unsubscripted G represents the total mass flux of the mixture.

Conservation of momentum

The change in axial momentum of the two-phase mixture was considered for a differential control volume of length dz. The forces considered were due to gravity, pressure and wall shear with the following result:

$$\frac{d}{dz}(G_v u_v + G_l u_l) = -g\rho_m - \frac{dP}{dz} - \frac{2 f_{lt} G^2}{\rho_l D_h}\Phi_{lo}^2, \tag{4}$$

where the mixture density is

$$\rho_m = \rho_v(1-\varphi_l) + \rho_l \varphi_l. \tag{5}$$

The combination of two-phase friction multiplier Φ_{lo}^2 and friction factor f_{lt} in equation (4) is compatible with constitutive relations (to be discussed subsequently) to account for the axial friction force between the swirling two-phase flow and the duct wall.

The conservation of momentum was written along a streamline for a single, spherical, liquid drop in the swirling flow. Forces on the drop were included due to gravity, fluid drag, phase change, wall shear, and vapor pressure gradient. The swirl flow of interest to this study is induced by twisted-tape inserts in the flow stream. The tape-twist ratio Y is the axial length of 180° of twist divided by the duct diameter. In this case, the liquid (drop) tangential velocity is related to the liquid axial velocity by

$$u_{l\theta} = u_l\left(\frac{\pi}{2Y}\right). \tag{6}$$

The resultant liquid streamline velocity (swirl velocity)

u_{ls} is related to the liquid axial velocity by $u_{ls} = R_s u_l$ where the parameter R_s is

$$R_s = \sqrt{\left(1+\left(\frac{\pi}{2Y}\right)^2\right)}. \quad (7)$$

Using these velocities, the liquid momentum equation may be written as

$$\rho_l u_l R_s \frac{du_l}{dz} = -\frac{\rho_l g}{R_s} + \frac{3C_D\rho_v R_s^2}{4d}(u_v-u_l)^2 - \frac{1}{R_s}\frac{dP}{dz} - \frac{2R_s}{D_h\varphi_l}\left[\frac{G^2 f_{lt}}{\rho_l}\Phi_{lo}^2 - \rho_v u_v^2 f_{vs}(1-\varphi_l)\right] - \frac{(1-\eta)R_s(u_v-u_l)}{\varphi_l}\frac{dG_v}{dz}. \quad (8)$$

The evaporation force in equation (8) is divided between the liquid and vapor phases by the parameter η, and the influence of the choice for η is discussed subsequently. All terms in equation (8) involve the parameter R_s which invokes the swirl velocity for this streamline momentum equation. The wall friction term is the second line of equation (8), where the axial force in square brackets is due to friction between drops and the duct wall. Consistent with constitutive relations employed, the first term gives the axial force for the swirling two-phase mixture, and subtracting the axial force due to the vapor swirl flow gives the drop contribution. The friction factor f_{vs} produces an axial force due to the swirling vapor with mass flux G_v. The force was projected along a streamline using the R_s parameter. (Note that the two-phase multiplier chosen for the mixture requires that f_{lt} be based on G and not on G_l.)

Conservation of energy

The steady state energy equation for the mixture was written in terms of the thermal energies of each phase and the heat supplied at the duct wall, q''. The condition of thermodynamic nonequilibrium between the phases was included. The liquid was assumed to be saturated while the vapor was superheated. The general result is

$$-c_{pl}G_l\frac{dT_{sat}}{dP}\frac{dP}{dz} + [i_{lv}+c_{pv}(T_v-T_{sat})]\frac{dG_v}{dz} + c_{pv}G_v\frac{dT_v}{dz} = q''\left(\frac{\pi D}{A}\right). \quad (9)$$

The second term in equation (9) accounts for vapor superheat where the liquid temperature T_l is equal to the saturation temperature T_{sat} corresponding to the local pressure.

The conservation of energy was written for the liquid drops flowing through a differential control volume. As the drops pass through the volume, a pressure reduction results in a change in temperature of the liquid. The liquid that is evaporated, dW_v, is raised to the superheated vapor temperature T_v. Heat is added to the drops through the vapor and directly from the duct wall. The conservation of energy for this case is

$$-c_{pl}G_l\frac{dT_{sat}}{dP}\frac{dP}{dz} + [i_{lv}+c_{pv}(T_v-T_{sat})]\frac{dG_v}{dz} = \frac{h_{l-w}\pi D\varphi_l}{A}(T_w-T_{sat}) + \frac{6h_{l-v}\varphi_l}{d}(T_v-T_{sat}). \quad (10)$$

The boundary condition at the heated wall is in terms of the known heat flux $q''(z)$. Heat is transferred from the wall to both the vapor and the drops and is given as follows:

$$q'' = h_{v-w}(1-\varphi_l)(T_w-T_v) + h_{l-w}\varphi_l(T_w-T_{sat}). \quad (11)$$

Solution arrangement

The conservation equations were applied to the two-phase flow downstream from the critical heat flux under forced convection swirling conditions. The application of the analysis to the prediction of experimental data involved inputing the parameters of mass flow rate, local heat flux q'' in the post-CHF region, and the conditions at CHF. Since most experiments do not include a measurement of vapor superheat, the primary parameter used for comparison with data is the wall temperature T_w which is obtained by rearranging equation (11):

$$T_w = \frac{h_{v-w}T_v(1-\varphi_l) + h_{l-w}T_l\varphi_l + q''}{h_{v-w}(1-\varphi_l) + h_{l-w}\varphi_l}. \quad (12)$$

The governing equations are then the continuity equations, (1)–(3), the momentum equations, (4) and (8), the energy equations, (9) and (10), and the boundary condition, equation (12). The unknowns are the mass fluxes G_v and G_l, the species velocities u_v and u_l, the drop volume fraction φ_l, the fluid pressure P, and the wall and vapor temperatures T_w and T_v. The four variables G_v, u_l, P and T_v were determined from the simultaneous solution of differential equations (4), (8), (9) and (10). Three of the remaining variables, G_l, u_v, and φ_l, were determined from the solution of algebraic equations (1)–(3), and T_w was found from equation (12).

Arrangement of the equations for solution required the differentiation of equations (1) and (2) and rearrangement to eliminate derivatives of φ_l and u_v. The four variables P, G_v, u_l and T_v were redefined for convenience as J_1, J_2, J_3 and J_4, respectively. A prime superscript used on these variables implies differentiation with respect to the independent variable z. After these changes, the mixture momentum equation, (4), becomes

$$\left[1-\frac{J_2^2}{\rho_v^2(1-\varphi_l)}\left(\frac{\partial\rho_v}{\partial P}\right)_{T_v}\right]J_1' + \left[\frac{2J_2}{\rho_v(1-\varphi_l)} - \frac{J_2^2}{\rho_v\rho_l(1-\varphi_l)^2 J_3} - J_3\right]J_2'$$

$$+\left[(G-J_2)\left(1-\frac{J_2^2}{\rho_v\rho_l(1-\varphi_l)^2J_3^2}\right)\right]J_3'$$

$$-\left[\frac{J_2^2}{\rho_v^2(1-\varphi_l)}\left(\frac{\partial\rho_v}{\partial T_v}\right)_P\right]J_4' = -g\rho_m - \frac{2f_{lt}G^2}{\rho_l D_h}\Phi_{lo}^2. \quad (13)$$

In a similar manner, the drop momentum equation, (8), becomes

$$\left[\frac{1}{R_s}\right]J_1' + \left[\frac{(1-\eta)R_s}{\varphi_l}\left(\frac{J_2}{\rho_v(1-\varphi_l)} - J_3\right)\right]J_2' + [\rho_l J_3 R_s]J_3'$$

$$= -\frac{\rho_l g}{R_s} + \frac{3C_D\rho_v R_s^2}{4d}\left(\frac{J_2}{\rho_v(1-\varphi_l)} - J_3\right)^2$$

$$-\frac{2R_s}{D_h\varphi_l}\left[\frac{G^2 f_{lt}}{\rho_l}\Phi_{lo}^2 - \frac{J_2^2 f_{vs}}{\rho_v(1-\varphi_l)}\right]. \quad (14)$$

Using variables J_1–J_4, the mixture energy equation, (9), becomes

$$-\left[c_{pl}(G-J_2)\frac{dT_{sat}}{dP}\right]J_1' + [i_{lv} + c_{pv}(J_4 - T_{sat})]J_2'$$

$$+[c_{pv}J_2]J_4' = q''\left(\frac{\pi D}{A}\right) \quad (15)$$

and the drop energy equation, (10), is

$$-\left[c_{pl}(G-J_2)\frac{dT_{sat}}{dP}\right]J_1' + [i_{lv} + c_{pv}(J_4 - T_{sat})]J_2'$$

$$= \frac{h_{l\,w}\pi D\varphi_l}{A}(T_w - T_{sat}) + \frac{6h_{l\,v}\varphi_l}{d}(J_4 - T_{sat}). \quad (16)$$

Equations (13)–(16) were solved simultaneously for J_1–J_4 using a matrix inversion algorithm to determine values of J_1'–J_4' as a function of z for input to a fourth-order Runge–Kutta algorithm.

Constitutive relations

Constitutive relations were adopted from the engineering literature for use with the analysis. The drop drag coefficient C_D was used as employed by Koizumi *et al.* [5], which accounts for the effects of drop evaporation on the drag force and is given as

$$C_D = \frac{1}{1 + \dfrac{c_{pv}(T_v - T_{sat})}{i_{lv}}}C_{DO} \quad (17)$$

with c_{pv} (and μ_l in equation (19)) based on $(T_v - T_{sat})/2$ and

$$C_{DO} = 24/Re_{l\,v} \qquad Re_{l\,v} \leqslant 2$$

$$= 18.5/Re_{l\,v}^{0.6} \qquad 2 < Re_{l\,v} \leqslant 500$$

$$= 0.44 \qquad Re_{l\,v} \geqslant 500 \quad (18)$$

where the Reynolds number is based on the relative velocity between the drops and the vapor:

$$Re_{l\,v} = \frac{(u_v - u_l)d}{\mu_l}. \quad (19)$$

Single-phase swirl flow friction factors f_{lt} and f_{vs} developed by Lopina and Bergles [6] were adopted along with the two-phase friction multiplier Φ_{lo}^2 developed by Reedy *et al.* [7]. Jensen *et al.* [8] used this combination of single and two-phase results successfully for a steam generator application with mass flux $G > 475$ kg m^{-2} s^{-1}. The relations are:

$$\frac{f_{lt}}{f_l} = \frac{f_{vs}}{f_v} = 2.75Y^{-0.406} = \frac{(4Y^2+\pi^2)^{3/2}}{8Y^3} \qquad Y \geqslant 11.25 \quad (20)$$

$$\Phi_{lo}^2 = 1 + X_{eq}\left(\frac{\rho_l}{\rho_v} - 1\right)C$$

$$C = 1.02X_{eq}^{-0.175}G^{-0.45} \qquad P > 4.1\text{ MPa}$$

$$= 0.357(1 + 10P_R)X_{eq}^{0.175}G^{-0.45}$$

$$2.1 \leqslant P \leqslant 4.1\text{ MPa}, \quad (21)$$

where the mass flux G has units of lbm h^{-1} ft^{-2} in equation (21), and f_l and f_v in equation (20) are single-phase axial flow friction factors given by the Blasius equation $f = 0.079/Re^{0.25}$.

The heat transfer coefficient between the heated wall and the vapor in a swirling flow, $h_{v\,w}$, was considered by comparing the correlations of Thorsen and Landis [9] and Lopina and Bergles [6] with superheated vapor data from the high pressure water experiments [4]. Based on these comparisons, the result of Lopina and Bergles was adopted, which is:

$$h_{v\,w} = \frac{k_v}{D_h}0.023(Re_v R_s)^{0.8}Pr_v^{0.4}$$

$$+\frac{k_v}{D_h}0.193\left[\left(\frac{Re_v}{Y}\right)^2\left(\frac{D_h}{D}\right)\beta(T_w - T_v)Pr_v\right]^{1/3}. \quad (22)$$

The heat transfer between the vapor and the liquid drops, $h_{v\,l}$, was modeled by Rohsenow and coworkers, who applied the correlation of Yuen and Chen [10]. This work was modified by Koizumi *et al.* [5] considering a significant amount of experimental data. The final modification of Koizumi was used in the present analysis as

$$\frac{h_{l\,v}}{\ln(1+B)/B}$$

$$= \frac{k_v}{d}(2 + 0.444\,Re_{l\,v} + 0.0875\,Re_{l\,v}^2) \qquad Re_{l\,v} \leqslant 0.1$$

$$= \frac{k_v}{d}(2 + 0.26\,Re_{l\,v}^{0.725}) \qquad 0.1 < Re_{l\,v} \leqslant 10$$

$$= \frac{k_v}{d}(2 + 0.328\,Re_{l\,v}^{0.59}) \qquad Re_{l\,v} > 10. \quad (23)$$

The constitutive relations discussed thus far are relatively well established and apply well to the situation of present interest. Models for direct heat transfer between the drops and the heated wall, however, are less established, and the databases available in the literature are generally based on high wall-superheat.

This condition inhibits direct drop-wall heat transfer to the extent that its effect has justifiably been neglected in many related investigations. For the low wall-superheat application of interest, the drop-wall heat transfer was included. Models due to Wachters *et al.* [11–13], Iloeje *et al.* [14], Yoder and Rohsenow [15], Groeneveld [16], and Baumeister *et al.* [17] were considered and tested in the analysis. By far the best results were obtained with a modification to the Baumeister model as adopted by Bergles *et al.* [3] and given by

$$h_{\mathrm{l\,w}} = 1.1\left[\frac{k_{\mathrm{v}}^3 i_{\mathrm{lv}}^* a \rho_{\mathrm{l}} \rho_{\mathrm{v}}}{(T_{\mathrm{w}} - T_{\mathrm{sat}})\,\mu_{\mathrm{v}}(\pi/6)^{1/3}}\right]^{1/4} \times \left[\frac{(1-X_{\mathrm{eq}})(6/\pi)}{X_{\mathrm{eq}}(\rho_{\mathrm{l}}/\rho_{\mathrm{v}}-1)+1}\right]^{2/3} \frac{\pi}{4} F, \quad (24)$$

where

$$i_{\mathrm{lv}}^* = \frac{i_{\mathrm{lv}}}{\left[1+\dfrac{7c_{\mathrm{pv}}(T_{\mathrm{w}}-T_{\mathrm{sat}})}{20 i_{\mathrm{lv}}}\right]^3}. \quad (25)$$

All properties in equation (24) were evaluated at the film temperature, and the radial drop acceleration due to the twisted tape is

$$a = \frac{(u_{\mathrm{l}}\pi)^2}{2dY^2}. \quad (26)$$

The factor F in equation (24) accounts for the radial force on the drop and was found [1] to be a function of a/g for data correlation purposes. Further details of the solution method are given by Chang [18].

MEASUREMENTS

Low wall-superheat heat transfer data in the post-CHF region with twisted-tape inserts were reduced from measurements [4] of heat transfer experiments to the two-phase flow of high pressure water, 16.0 ± 0.1 MPa. The test section was a 13.1 m long vertical tube with a 10 mm inside diameter. Water flowed upwards inside of the tube, and heat was supplied by liquid sodium flowing counter-current in the surrounding annulus. Water entered the test section subcooled in all cases. Tests chosen for use in this study exhibited a clear post-CHF region consisting of five or more axial measurement points. All of the seven tests selected had vapor superheat at the test section exit such that the entire post-CHF region was present in the test section at steady-state.

The mass fluxes of all of the experiments were in a high range, above 910 kg m^{-2} s^{-1}. On a relative basis, they can be divided into a low category of 910 kg m^{-2} s^{-1}, an intermediate level of 1300 ± 80 kg m^{-2} s^{-1} and a high category of 1850 ± 30 kg m^{-2} s^{-1}. The data selected were comprised of experiments with three twisted tape inserts: $Y = 2.51$, 5.02 and 7.53.

Application of model to data

The model presented was applied to the high-pressure post-CHF water swirl flow data with calculations starting at the measured CHF position. Initial conditions at CHF were the experimental pressure and equilibrium quality. It was assumed that the drops and vapor were in thermodynamic equilibrium at CHF with the initial drop diameter, d, determined from a critical Weber number of $We = \bar{\rho}_{\mathrm{v}} \times (u_{\mathrm{v}} - u_{\mathrm{l}})^2 d/\sigma = 7.5$. A value of 6.5 was used in high-speed drop/gas flows [19], and other researchers [15, 20–22] used critical Weber numbers in the range of $6.5 \sim 7.5$. The effect on results of this choice is discussed subsequently. The total mass flux G and the radial heat flux along the test section in the post-CHF region were input from the experiments. Finally, an initial slip, $S = u_{\mathrm{v}}/u_{\mathrm{l}}$, at CHF was required to start the solution. The choice of this parameter is also discussed subsequently in the Results and Discussion section. The drop volume fraction φ_{l} (or the void fraction α) was then calculated from

$$\alpha = 1 - \varphi_{\mathrm{l}} = \frac{1}{1 + \dfrac{S}{\left(\dfrac{X}{1-X}\right)\left(\dfrac{\rho_{\mathrm{l}}}{\rho_{\mathrm{v}}}\right)}}. \quad (27)$$

The mathematical solution to equations (13)–(16) for unknowns P, G_{v}, u_{l} and T_{v} was accomplished by a variable step Runge–Kutta algorithm with global error specification. The solution progressed downstream from CHF with variables G_{l}, φ_{l}, u_{v} and T_{w} calculated from algebraic relations equations (1)–(3) and equation (12) after each step. The actual quality was then found from equation (27) and the saturation temperature T_{sat} from the pressure. The drop number density, $N = 6\varphi_{\mathrm{l}}/\pi d^3$, was set at CHF by the initial drop diameter and the equilibrium liquid volume fraction. If at any downstream location the calculated drop diameter d was such that the critical Weber number was exceeded, the drop number density N was doubled, and the drop diameter was recalculated.

RESULTS AND DISCUSSION

Typical results

Reduced data from a typical test are shown as square symbols in Fig. 1 for an intermediate value of mass flux and the smallest tape-twist ratio, $G = 1222$ kg m^{-2} s^{-1} and $Y = 2.51$, respectively. The experimental tube wall temperatures at the boiling water surface are plotted in the direction of the water flow. The CHF location (open symbol) is shown to occur approximately 6 m downstream of the test section inlet, and the solid symbols represent wall temperatures in the post-CHF region extending for a length of 1 m downstream and terminating with an actual quality approaching 1.0.

The prediction of the inner water-tube wall temperature is shown as the solid line in Fig. 1. The

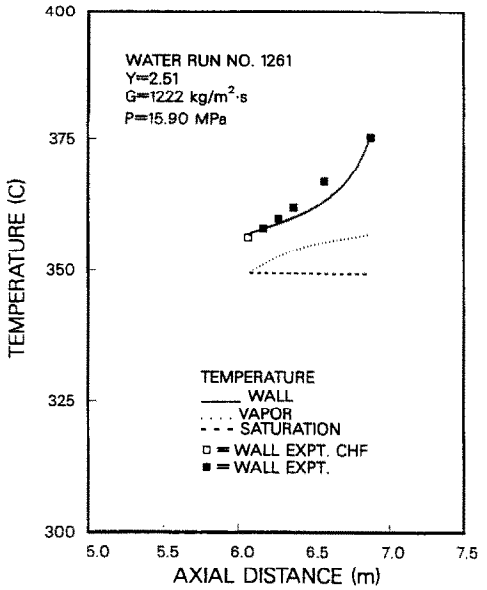

FIG. 1. Typical data comparison at smallest $Y = 2.51$ and intermediate $G = 1222$ kg m^{-2} s^{-1}.

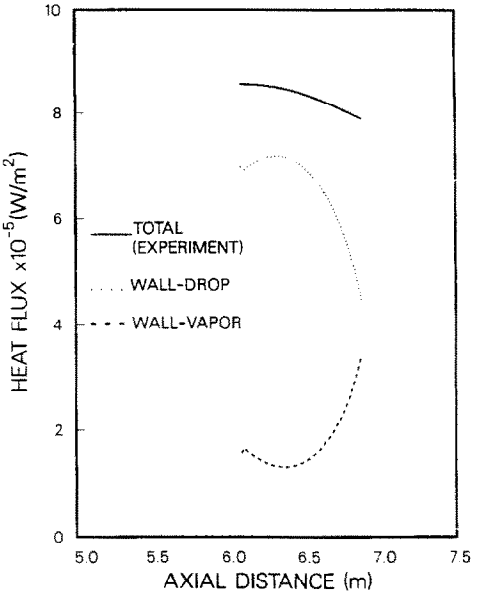

FIG. 3. Heat transfer division at smallest $Y = 2.51$ and intermediate $G = 1222$ kg m^{-2} s^{-1}.

predictions are in good agreement with the data in both magnitude and trend. The results also show that the saturated liquid drop temperature changed very little in the post-CHF region due to the small pressure drop there, and the vapor was superheated by about 10°C at the exit of the region. Although this vapor superheat is relatively low due to the liquid heating aspect of the experiments, it is an important phenomenon and is inherent in the developed model.

The prediction of the degree of nonequilibrium is also shown in Fig. 2 as the deviation of the predicted actual quality from the experimental equilibrium quality. In this experiment, the quality at CHF is approximately 0.8 (equilibrium = actual), and the equilibrium quality is about 6% above the actual quality at the end of the post-CHF region.

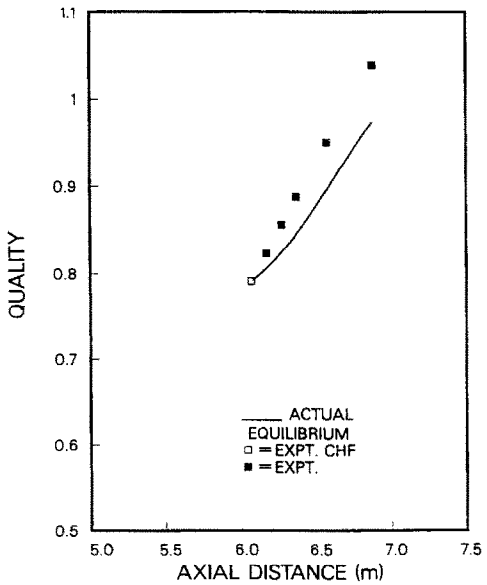

FIG. 2. Qualities at smallest $Y = 2.51$ and intermediate $G = 1222$ kg m^{-2} s^{-1}.

Shown in Fig. 3 for the same experiment as Figs. 1 and 2 is the wall heat flux division between vapor and drops. Initially the drop contribution is large, but it decreases towards zero rapidly due to decreasing drop size and increasing wall superheat. In all of the experiments [4], the high mass fluxes and low wall-superheats combined to produce relatively large drop-wall contributions to the heat transfer at least initially just downstream of CHF. This result is in contrast to drop-wall heat transfer that is generally much smaller for high wall-superheat conditions.

The contribution to the heat transfer of the wall–vapor interchange has the opposite trend as the drop contribution. Shown in Fig. 3 is the increasing contribution of the vapor which will equal the total heat transfer when the actual quality $X = 1$.

Fluid mechanics of the experiment of Figs. 1–3 are shown in Fig. 4. It is seen that the vapor accelerates in the flow direction in the post-CHF region as the quality increases, and the drops are accelerated by the vapor. The slip ratio is seen in Fig. 4 to increase in the flow direction, but the amount of increase is small. The discontinuities in slope of the drop velocity and slip ratio curves of Fig. 4 are due to the numerical algorithm used that breaks up each drop into two smaller drops of equal size whenever the critical Weber number is reached. This procedure was adopted from the work of Yoder and Rohsenow [15].

Tape-twist ratio effect

The results shown in Figs. 5–7 correspond to Figs. 2–4 having a similar mass flux and a considerably

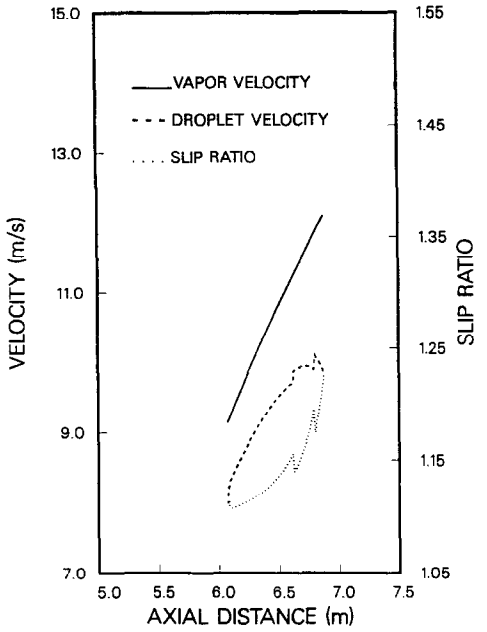

FIG. 4. Phase velocities at smallest $Y = 2.51$ and intermediate $G = 1222$ kg m^{-2} s^{-1}.

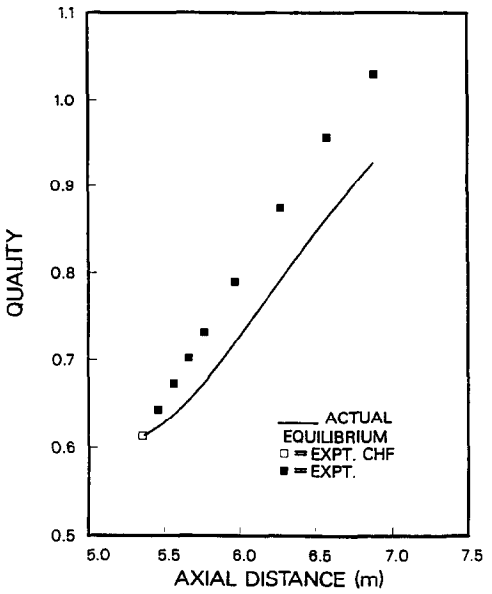

FIG. 6. Degree of nonequilibrium at largest $Y = 7.53$ and intermediate $G = 1380$ kg m^{-2} s^{-1}.

larger tape-twist ratio. The mass flux of the experiment of Figs. 5–7 is $G = 1380$ kg m^{-2} s^{-1}, and $Y = 7.53$. The smaller swirl effect of the larger tape-twist ratio of 7.53 reduces the effectiveness of the heat transfer, and the post-CHF region is seen to extend for a longer distance (~ 1.5 m) downstream of CHF. The data trends of the heat flux contributions of Fig. 5 and the qualities of Fig. 6 are similar to those of Figs. 2 and 3, respectively, although the magnitudes differ. The drop velocity of Fig. 7 parallels the vapor, consequently, the slip ratio is nearly constant in the whole post-CHF region. The results of a third experiment at the same mass flux and $Y = 5.02$ fell between the slip ratio results of Figs. 4 and 7, and other parametric trends were similar to Figs. 2 and 3, and 5 and 6.

In general it can be said that at this intermediate mass flux and three different tape-twist ratios, the thermodynamic nonequilibrium phenomenon is approximately the same based on the vapor superheats. (The wall superheat is higher at larger tape-twist ratios as expected due to the reduction in heat transfer coefficient.) The drop-wall heat transfer

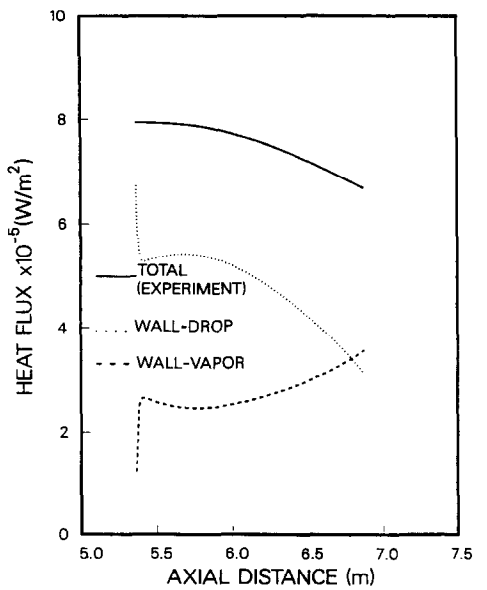

FIG. 5. Heat transfer at largest $Y = 7.53$ and intermediate $G = 1380$ kg m^{-2} s^{-1}.

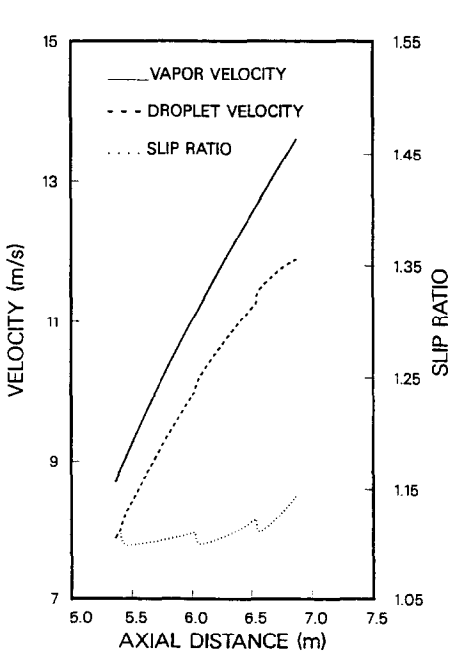

FIG. 7. Near constant slip at largest $Y = 7.53$ and intermediate $G = 1380$ kg m^{-2} s^{-1}.

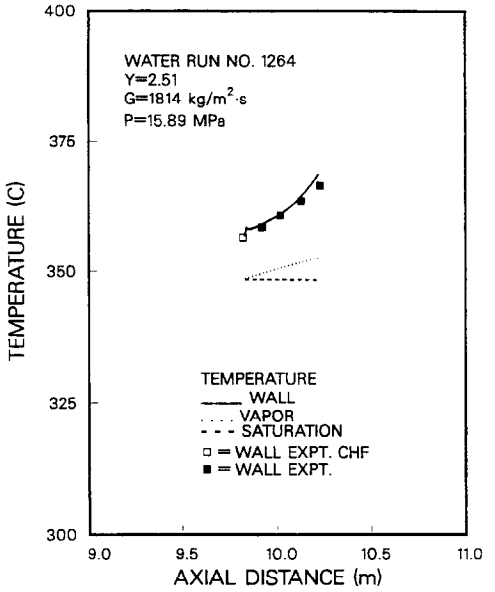

FIG. 8. Data comparison at smallest $Y = 2.51$ and largest $G = 1814$ kg m^{-2} s^{-1}.

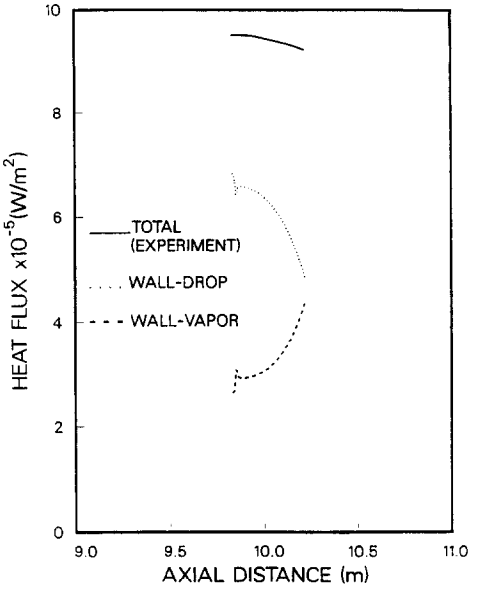

FIG. 9. Heat transfer at smallest $Y = 2.51$ and largest $G = 1814$ kg m^{-2} s^{-1}.

decreases with the smaller swirl effect produced by larger values of Y. As the quality increases, the heat flux from the wall to the vapor increases significantly, but the temperature of the vapor does not. This result indicates that the vapor-to-drop heat transfer becomes more important at higher qualities in the post-CHF region.

Mass flux effect

The effect of mass flux on the results was compared at $Y = 2.51$ and $G = 1222$ kg m^{-2} s^{-1} (Figs. 1–4), $G = 1814$ kg m^{-2} s^{-1} (Figs. 8 and 9) and $G = 910$ kg m^{-2} s^{-1} (Fig. 10). At the highest mass flux, the vapor superheat is seen in Fig. 8 to decrease from the intermediate mass flux case of Fig. 1. The same twisted-tape insert was used in both experiments, and the total local heat fluxes were similar. The reduction in vapor superheat is attributable to increased effectiveness of drop-vapor heat transfer. The total heat transfer is seen to increase somewhat in Fig. 9 compared to Fig. 3, due primarily to increased wall-to-vapor heat transfer.

The lowest mass flux of 910 kg m^{-2} s^{-1} at $Y = 2.51$ produced parameter trends similar to the intermediate and high mass flux results. The low mass flux, like the larger tape-twist ratio results of Fig. 7, produced small radial accelerations and a near constant slip ratio in the post-CHF region. The difference between actual and equilibrium quality was similar to Fig. 2, but the quality at CHF was much lower at $X = 0.45$. The increased mass of liquid in the initial post-CHF region produced good drop-wall heat transfer, while the low swirl effect reduced the vapor-wall heat transfer as shown in Fig. 10 as compared to the results of Figs. 3 and 9.

Final parameters

All of the predictions presented in the preceding discussion incorporated an initial value of the velocity slip ratio S at CHF, a critical Weber number of 7.5, a value for the apportionment of the evaporation force, η, and a relation for the effect of radial drop acceleration on drop-wall heat transfer described by the parameter $F(a/g)$ in equation (24). The F factor was the final constitutive relation needed to complete the model. In the general data correlation work [1], it was found that although both the mass flux and tape-twist ratio affected the drop-wall heat transfer, their

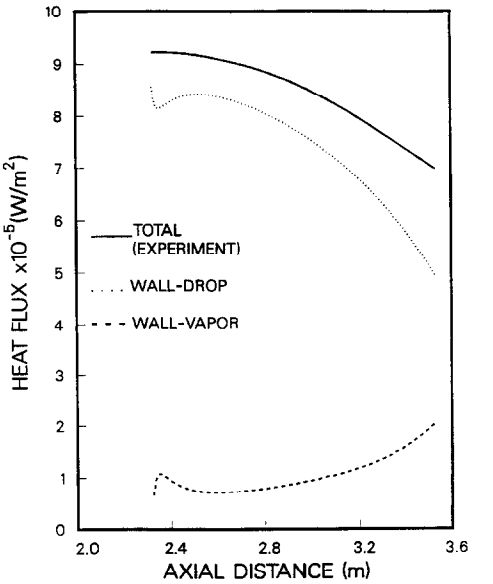

FIG. 10. Heat transfer at smallest $Y = 2.51$ and smallest $G = 910$ kg m^{-2} s^{-1}.

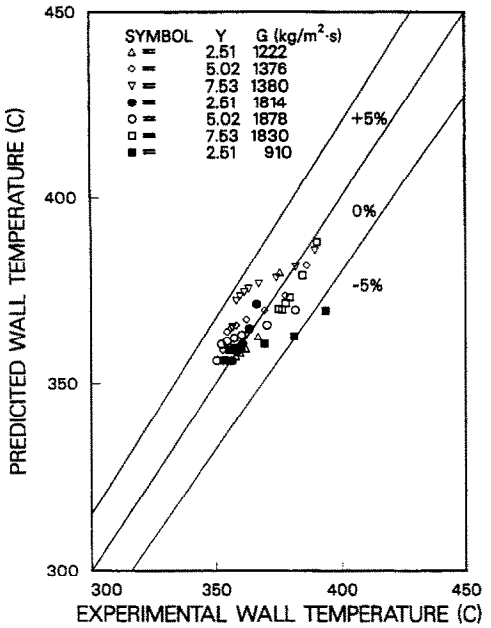

FIG. 11. Predictions of all data.

influence was through the common parameter of drop radial acceleration, a. A form of F that correlated the data in this general way was $F \propto (a/g)^{\lambda}$. Consequently, in the present study, a relation for $F(a/g)$ used in equation (24) was developed from the data as

$$F(a/g) = 4.6\left(\frac{a}{g}\right)^{0.4}. \tag{28}$$

The effects of critical Weber number and the slip at CHF on the calculated results were tested. No significant changes in results were found for a large range of We including the 6.5 to 7.5 range and for initial slip at CHF in the range of $1.05 \leqslant S \leqslant 1.5$. Thus, $We = 7.5$ and $S = 1.1$ at CHF were used with the model in all cases.

The effect of the apportionment of the phase change force between the drops and the vapor was investigated through the parameter η. Test cases were run with η at its extreme values of 0 and 1 and at the mean value of 0.5. Results for pressure and velocities predictions were almost unchanged, showing that this force was small compared to the others acting in the flow. Thereafter, all computations were made with $\eta = 0.5$.

Test runs were also performed with regard to numerical step size. The predictions were always found to be repeatable within four significant figures.

Composite data prediction

All of the experimentally determined tube-wall temperatures are compared to predictions of the present model in Fig. 11 for all mass fluxes and all tape-twist ratios. The good agreement serves as an overall verification of the model with the constitutive relations used.

CONCLUSIONS

A mathematical model of two-phase dispersed swirl flow was developed. Predictions derived from this model were verified by comparisons with experimental data in the post-CHF region of high-pressure water with swirl induced by twisted-tape inserts. Good agreement was obtained in magnitude and trend on an overall and local basis.

The data used for model verification were obtained from a heat exchanger application with low wall-superheat, high mass flux and a range of tape-twist ratios as low as $Y = 2.51$. Predictions from the model showed these conditions combined to produce significant direct heat transfer between the drops in the flow and the heated tube wall in the region just downstream of CHF. This contribution to heat transfer declined substantially thereafter as the vapor-wall heat transfer increased; however, the total effect of the drops was considerable compared to high wall-superheat applications (above 100°C).

Thermodynamic nonequilibrium inherent in the model predicted small vapor superheat of approximately 10°C in most tests. Experiments with higher heat fluxes which could have produced larger vapor superheats showed better vapor-to-drop heat transfer. The nonequilibrium was also evident from the difference between the equilibrium and actual quality which reached approximately 6% as the equilibrium quality approached unity.

Small radial acceleration of the flow, caused by both large tape-twist ratio or low mass flux, produced near constant axial vapor and drop accelerations resulting in near constant slip ratios in the entire post-CHF region.

REFERENCES

1. P. Papadopoulos, D. M. France and W. J. Minkowycz, Heat transfer to dispersed swirl flow of high pressure water with low wall-superheat, *Expl Heat Transfer* **4**, 153–169 (1991).
2. P. Papadopoulos, D. M. France, W. J. Minkowycz, J. Harty, M.-S. Wu and M. N. Hamoudeh, Two-phase dispersed flow heat transfer augmented by twisted tapes, *J. Enhanced Heat Transfer* (in press).
3. A. E. Bergles, W. D. Fuller and S. J. Hynek, Dispersed flow film boiling of nitrogen with swirl flow, *Int. J. Heat Mass Transfer* **14**, 1343–1354 (1971).
4. R. D. Carlson, D. M. France, M. J. Gabler, K. Kim and W. Veljovich, Heat transfer augmentation in liquid metal reactor steam generators, *Proceedings of the 1986 Joint ASME/ANS Nuclear Power Conference*, pp. 211–217. American Nuclear Society, Hinsdale, IL (1986).
5. Y. Koizumi, T. Ueda and H. Tanaka, Post dryout heat transfer to R-113 upward flow in a vertical tube, *Int. J. Heat Mass Transfer* **22**, 669–678 (1979).
6. R. F. Lopina and A. E. Bergles, Heat transfer and pressure drop in tape-generated swirl flow of single-phase water, *J. Heat Transfer* **91**, 434–442 (1969).
7. D. G. Reddy, S. R. Sreepada and A. N. Nahavandi,

Two-phase friction multiplier correlation for high-pressure steam water flow, EPRI NP-2522, Electric Power Research Institute, Palo Alto, California (1982).
8. M. W. Jensen, M. Pourdashti and H. P. Bensler, Two-phase pressure drop with twisted tape swirl generator, *Int. J. Multiphase Flow* **11,** 201–211 (1983).
9. R. Thorsen and F. Landis, Friction and heat transfer characteristics in turbulent swirl flow subjected to large transverse temperature gradients, *J. Heat Transfer* **90,** 87–97 (1968).
10. M. C. Yuen and L. W. Chen, Heat transfer measurement of evaporating liquid droplets, *Int. J. Heat Mass Transfer* **21,** 537–542 (1978).
11. L. H. J. Wachters, H. Bonne and H. J. Van Nouhuis, The heat transfer from a hot horizontal plate to sessile water drops in the spheroidal state, *Chem. Engng Sci.* **21,** 923–936 (1966).
12. L. H. J. Wachters, L. Smulders, J. R. Vermeulen and H. C. Kleiweg, The heat transfer from a hot wall to impinging mist droplets in the spheroidal state, *Chem. Engng Sci.* **21,** 1231–1238 (1966).
13. L. H. J. Wachters and N. A. J. Westerling, The heat transfer from a hot wall to impinging water drops in the spheroidal state, *Chem. Engng Sci.* **21,** 1047–1056 (1966).
14. O. C. Iloeje, D. K. Plummer, W. M. Rohsenow and P. Griffith, A study of wall rewet and heat transfer in dispersed vertical flow, MIT Technical Report 72718-92 (1974).
15. G. L. Yoder and W. M. Rohsenow, A solution for dispersed flow heat transfer using equilibrium fluid condition, *J. Heat Transfer* **105,** 10–17 (1983).
16. D. C. Groeneveld, The thermal behavior of a heated surface at and beyond dryout, AECL-4309 (1972).
17. K. J. Baumeister, T. D. Hamill and G. J. Schoessow, A generalized correlation of vaporization times of drops in film boiling on a flat plate, *Proceedings of the Third International Heat Transfer Conference*, Vol. IV, pp. 66–73. A.I.Ch.E. (1966).
18. C. Chang, Heat transfer analysis of two-phase dispersed swirl flow, Ph.D. Thesis, University of Illinois, Chicago, Illinois (1991).
19. N. Isshiki, Theoretical and experimental study on atomization of liquid drop in high speed gas stream, Transportation Technical Research Institute Report 35, Tokyo, Japan (1968).
20. R. P. Forslund and W. M. Rohsenow, Thermal non-equilibrium in dispersed flow film boiling in a vertical tube, MIT Technical Report 75312-44 (1966).
21. D. C. Groeneveld, The thermal behavior of a heated surface at and beyond dry-out, Chalk River Nuclear Laboratories Report AECL-4309, Chalk River, Ontario, Canada (1972).
22. D. N. Plummer, P. Griffith and W. M. Rohsenow, Post-critical heat transfer to flowing liquid in a vertical tube, *16th National Heat Transfer Conference*, St. Louis, Missouri (1976).